ACS OMEGA

Article

Cite This: ACS Omega 2018, 3, 8401−8407

http://pubs.acs.org/journal/acsodf

Key Residues for the Formation of Aβ42 Amyloid Fibrils

Frederick Hsu,† Giovanna Park,† and Zhefeng Guo*

Department of Neurology, Brain Research Institute, Molecular Biology Institute, University of California, 710 Westwood Plaza, Los Angeles, California 90095, United States

ABSTRACT: Formation of amyloid fibrils by Aβ42 protein is a pathological hallmark of Alzheimer's disease. Aβ42 fibrillization is a nucleation-dependent polymerization process, in which nucleation is the rate-limiting step. Structural knowledge of the fibril nucleus is important to understand the molecular mechanism of Aβ aggregation and is also critical for successful modulation of the fibrillization process. Here, we used a scanning mutagenesis approach to study the role of each residue position in Aβ42 fibrillization kinetics. The side chain we used to replace the native residue is a nitroxide spin label called R1, which was introduced using site-directed spin labeling. In this systematic study, all residue positions of Aβ42 sequence were studied, and we identified six key residues for the Aβ42 fibril formation: H14, E22, D23, G33, G37, and G38. Our results suggest that charges at positions 22 and 23 and backbone flexibilities at positions 33, 37, and 38 play key roles in Aβ42 fibrillization kinetics. Our results also suggest that the formation of a β-strand at residues 15−21 is an important feature in Aβ42 fibril nucleus. In overall evaluation of all of the mutational effects on fibrillization kinetics, we found that the thioflavin T fluorescence at the aggregation plateau is a poor indicator of aggregation rates.

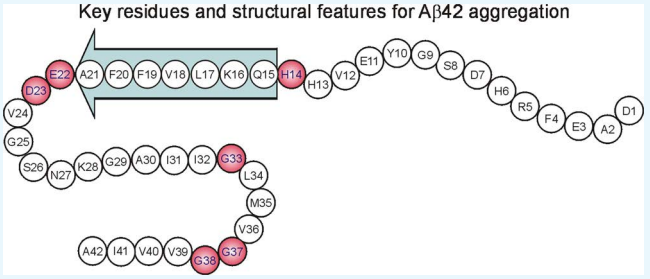

INTRODUCTION

Formation of amyloid fibrils is a key process underlying the pathogenesis of a wide range of human disorders, including Alzheimer's disease, Parkinson's disease, and type 2 diabetes.[1,2] The fibrillization process is a nucleation-dependent polymerization, in which nucleation is the rate-limiting step. The nucleation step is manifested as the lag phase of the sigmoidal aggregation curve, during which the fibril nucleus accumulates to exceed certain threshold concentrations and thus the elongation of fibril nuclei becomes the dominant process, leading to the formation of mature fibrils. In the last decade, significant progress has been made in the understanding of the microscopic aggregation processes.[3−5] It has been shown that both primary and secondary nucleation reactions may take place in the lag phase,[6,7] and determination of the nucleation rate is best achieved by global fitting of the aggregation data over a wide range of protein concentrations.[8,9] Regardless of the exact mechanism of aggregation, structural knowledge of the fibril nucleus is important for a complete understanding of the fibrillization process and is critical for successful design of fibrillization modulators.

Amyloid-β (Aβ) protein is the major component of amyloid plaques, a pathological hallmark of Alzheimer's disease.[10] There are two major variants of Aβ protein: Aβ40 and Aβ42. Although Aβ40 is severalfold more abundant than Aβ42 in the brain,[11−13] Aβ42 is the major component of the amyloid plaques.[14−17] Aβ aggregation and the structure of Aβ aggregates have been under intensive investigation. Several recent structural studies have produced detailed knowledge on the structure of the final aggregation product of Aβ42, the amyloid fibrils.[18−21] The structure of the Aβ42 fibril nucleus, in contrast, is still poorly understood.

To gain insights into the structure of Aβ42 fibril nuclei, here we used a scanning mutagenesis approach to study the role of each residue position in fibrillization kinetics. The rationale is that if a residue is of structural importance to the fibril nucleus, then mutation at that residue position may affect fibrillization in a dramatic way. Depending on whether a mutation is stabilizing or destabilizing the fibril nucleus, it will either promote or slow down fibrillization. The side chain we used to replace the native residue is a nitroxide spin label called R1 (Figure 1A), which was introduced using site-directed spin labeling.[22] Modeling of the spin label on a parallel β-sheet[23] suggests that the crystal structure of the spin label[24] can be accommodated in the amyloid core (Figure 1B). The use of spin label stems from our routine structural studies of spin-labeled Aβ42 aggregates using electron paramagnetic resonance spectroscopy.[25,26] Crystal structures of spin-labeled T4 lysozyme have shown that the R1 side chain is well tolerated in T4 lysozyme when labeled on a solvent-exposed helical site, but could cause local structural changes when introduced at the hydrophobic core.[27,28] In this systematic study, all residue positions of Aβ42 sequence were studied in aggregation kinetics experiments, and we identified six key residues for the Aβ42 fibril formation: H14, E22, D23, G33, G37, and G38. Our results also suggest the formation of a β-strand in the fibril nucleus at residues 15−21. The potential roles

Received: May 2, 2018
Accepted: July 17, 2018
Published: July 31, 2018

DOI: 10.1021/acsomega.8b00887
ACS Omega 2018, 3, 8401−8407

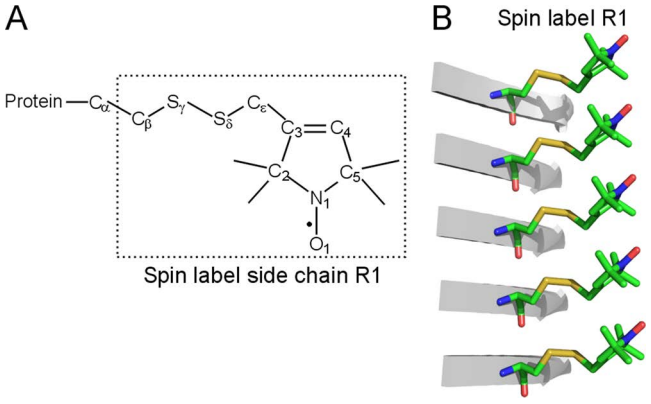

Figure 1. Structure of the spin label R1. (A) Chemical structure of R1. (B) Cartoon representation of the spin label R1 in a parallel in-register β-sheet. This model is based on the crystal structures of the NNQQNY peptide[23] and the spin labeling reagent 1-oxyl-2,2,5,5-tetramethylpyrroline-3-methyl methanethiosulfonate (MTSSL).[24]

of these structural features in the aggregation of Aβ42 are discussed.

RESULTS AND DISCUSSION

Formation of Aβ42 amyloid fibrils is a nucleation-dependent polymerization process. Structural knowledge of the fibril nucleus is important for the mechanistic understanding of Aβ fibrillization and also for structure-based intervention targeting the aggregation process. Here, we used the spin label R1 (Figure 1), a bulky hydrophobic side chain, to scan through the full sequence of Aβ42 and investigate the effect of spin label substitution on fibrillization kinetics. Because nucleation is a rate-limiting step, the free energy of the fibril nucleus is higher than those of both Aβ monomers and fibrils. Substitutions that lower the energy of the fibril nucleus would accelerate the rate of nucleation, whereas substitutions that destabilize the fibril nucleus would slow down the rate of nucleation and, consequently, the rate of fibrillization. The approach of proline scanning mutagenesis has been previously used to study the aggregation of Aβ42 by Morimoto et al.,[29] but the rate of aggregation was not determined for all residue positions. To our best knowledge, this work is the first report of a comprehensive study of fibrillization kinetics in combination with scanning mutagenesis at all 42 residue positions in the Aβ42 sequence.

The fibrillization kinetics of wild-type and 42 spin-labeled variants of Aβ42 were performed at 37 °C under quiescent conditions. Two Aβ42 concentrations at 5 and 10 μM were used in the first set of aggregation assays. The fibril formation was monitored with thioflavin T fluorescence. As shown in Figure 2, wild-type and most of the Aβ42 mutants show sigmoidal aggregation kinetics, typical of nucleation-dependent fibrillization. Six Aβ42 mutants did not show typical sigmoidal aggregation curves: H14R1, E22R1, D23R1, G33R1, G37R1, and G38R1. These six mutants are characterized by a very broad growth phase or no growth phase and very low thioflavin T amplitude at the end of the aggregation period (40 h). We then increased the Aβ concentration to 20 and 40 μM for these six mutants and repeated the aggregation experiments. As shown in Figure 3, the aggregation curves of H14R1, G33R1, G37R1, and G38R1 were restored to a more typical sigmoid shape, but E22R1 and D23R1 did not display sigmoidal curves even at these higher concentrations. Therefore, these results suggest that six residue positions, H14, E22, D23, G33, G37, and G38, are important for the nucleation-dependent polymerization of Aβ42 fibrils. Among these six residues, E22 and D23 are essential for the sigmoidal aggregation kinetics.

To quantitatively evaluate the effect of site-specific substitutions, we determined the half time of aggregation directly from the aggregation curves without relying on fitting to any specific sigmoidal functions. The half time is the time of aggregation at which the thioflavin T fluorescence has reached 50% of the fluorescence at the aggregation plateau. Even though we chose to use this type of rudimentary data analysis, our analysis is rooted in recent advances in the mechanistic understanding of protein aggregation. First, we chose to use half time, not lag time, as a measure of mutational effects on nucleation. As discussed previously by Arosio et al.,[7] primary nucleation is not the only microscopic process during the lag time of aggregation. Most notably, fibril-catalyzed secondary nucleation has been observed for the aggregation of Aβ42,[6] Aβ40,[30] and α-synuclein.[31] Whereas primary nucleation is the most active in the beginning of the lag phase, secondary nucleation would soon dominate and reach maximal rate near the half time of aggregation.[7] Therefore, half time is a better indicator for the overall nucleation rate when both primary and secondary nucleation reactions are present. Second, kinetic analysis has been shown to be a powerful approach to reveal detailed molecular events during the aggregation process.[32,33] A number of mathematical models have been used to fit the aggregation data.[3,34] For Aβ aggregation, experimental evidence also suggests a mechanism of nucleated conformational conversion,[35,36] which would add another layer of complexity to the mechanism of primary nucleation. It is not straightforward to obtain microscopic rate constants from kinetic data as similar kinetic profiles can be obtained from different mathematical models. In case of primary and secondary nucleation, this issue is alleviated by global fitting of the kinetic data over a wide range of protein concentrations.[8,9] And because our kinetic data consist of only two protein concentrations, we refrained from fitting of our data to specific kinetic models. The goal of this investigation is to obtain structural insights into the fibril nucleus, so data analysis aiming at understanding the aggregation mechanism is beyond the scope of this work. Third, half time of aggregation is not a direct measure of nucleation rate, as it can be affected by primary nucleation, secondary nucleation, fibril elongation, and fragmentation. In this study, fibril formation was performed under quiescent conditions, so fibril fragmentation is not the main driving force of aggregation rate. If we can assume that fibril elongation rate remains unchanged by mutagenesis, then the changes in half time of aggregation can be used to evaluate the effects on fibril nucleation, without distinguishing primary and secondary nucleation.

In Figure 4, we plot the half time of aggregation as a function of residue positions. The half time was not determined for the six mutants that did not show sigmoidal aggregation curves: H14, E22R1, D23R1, G33R1, G37R1, and G38R1. When looking at the overall pattern of residue-specific aggregation rate, we found that spin labeling at the N-terminal region (residues 1−10) did not lead to dramatic differences in the half time of aggregation from one residue to the next, suggesting that the N-terminal region may play a lesser role. We also observed that spin labeling at positions 16, 18, and 20 dramatically delayed Aβ42 aggregation, whereas spin labeling at positions 15, 17, 19, and 21 led to faster aggregation kinetics. The opposite effects on aggregation for alternating residue positions in this region suggest that residues 15−21 may adopt a β-strand structure,

DOI: 10.1021/acsomega.8b00887
ACS Omega 2018, 3, 8401−8407

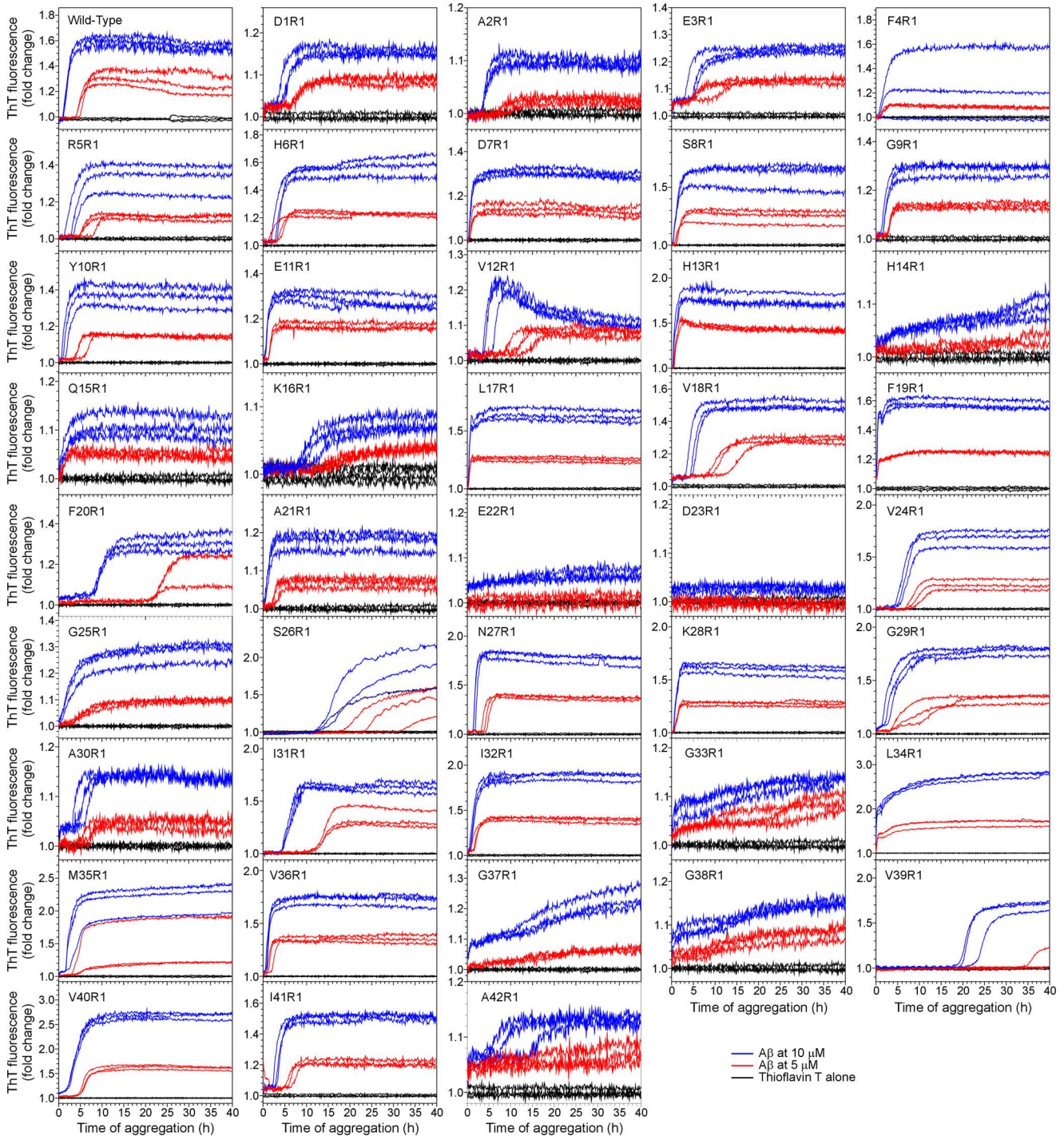

Figure 2. Aggregation kinetics of wild-type and 42 spin-labeled Aβ42 mutants. R1 represents the spin label. Aβ aggregation was performed at two concentrations, 5 and 10 μM, in phosphate-buffered saline (PBS) buffer (pH 7.4) at 37 °C without agitation.

which has a periodicity of two, in the fibril nucleus. In the recent high-resolution structures of Aβ42 fibrils based on cryoEM,[19] residues 15−21 adopt a β-strand structure, and the side chains of residues 15, 17, and 19 point inside the fibril core. This confirms the notion that spin labeling at the fibril core (such as residues 15, 17, 19, and 21) does not disrupt core packing in the fibril nucleus. It is not immediately clear why spin labeling at residues 16, 18, and 20, whose side chains point outside the amyloid core, delayed Aβ42 fibril formation.

In this work, we obtained a large dataset of Aβ42 aggregation kinetics, which allowed us to evaluate the overall relationship between the rate of aggregation and the thioflavin T fluorescence at the aggregation plateau. We have previously reported that thioflavin T fluorescence intensity is directly proportional to the amount of amyloid fibrils.[37] However, it is an open question whether thioflavin T fluorescence intensity is a representative measure of aggregation rate. Therefore, we plotted the thioflavin T fluorescence intensity at the aggregation plateau for the kinetics data versus the half time of aggregation for all of the spin-labeled Aβ42 mutants (Figure 5). Overall, these results show that there is not a clear correlation between thioflavin T fluorescence intensity and half time of aggregation.

DOI: 10.1021/acsomega.8b00887
ACS Omega 2018, 3, 8401−8407

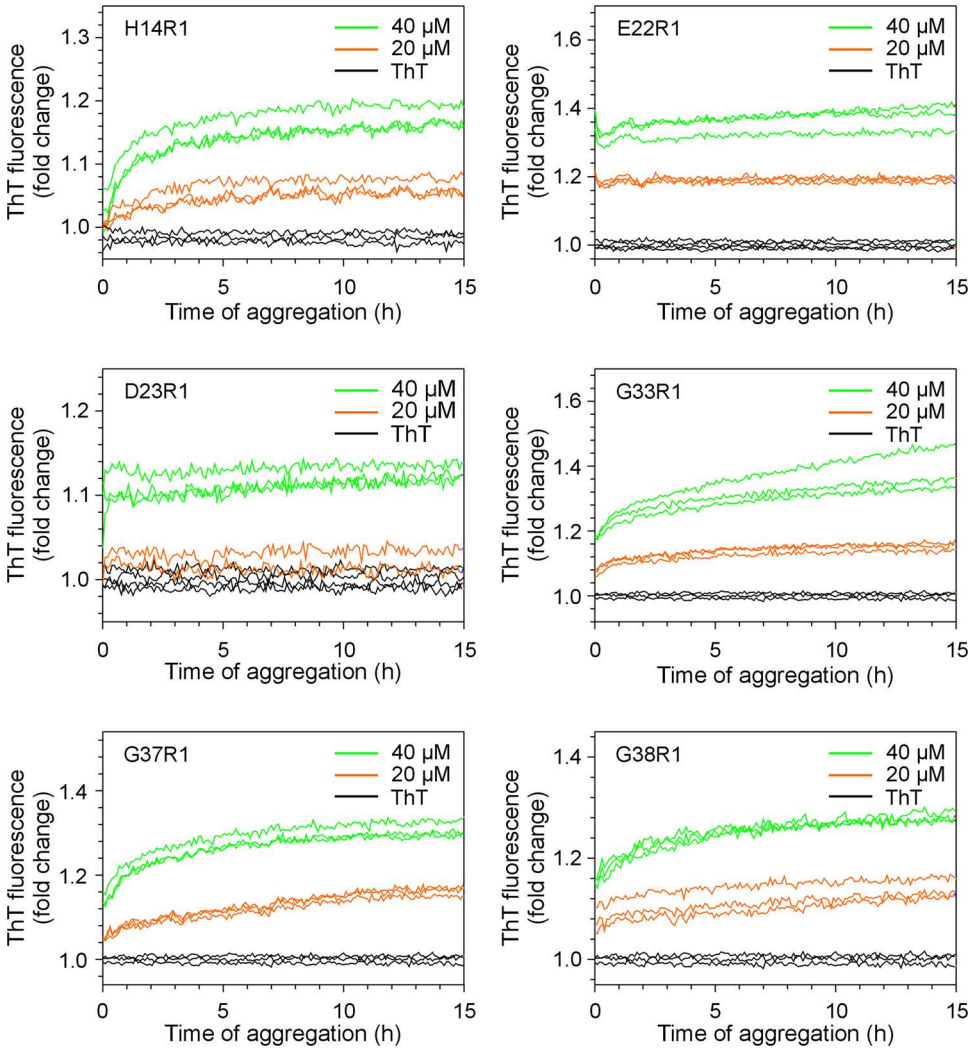

Figure 3. Aggregation kinetics of Aβ42 H14R1, E22R1, D23R1, G33R1, G37R1, and G38R1 at 20 and 40 μM. R1 represents the spin label. Aggregation was performed at 37 °C without agitation.

Therefore, when evaluating the effect of mutations on aggregation, it is preferable to use aggregation kinetics rather than simply the thioflavin T fluorescence at the end of aggregation.

Among the six residue positions that show aberrant aggregation kinetics upon spin labeling (Figure 6), two of them are charged residues: E22 and D23. There are nine charged residues in Aβ42 sequence: D1, E3, R5, D7, E11, K16, E22, D23, and K28. Because spin labeling at other charged residue positions shows only a mild effect on aggregation kinetics, the effect at E22 and D23 cannot be explained simply by changes in the isoelectric point of Aβ42. We also considered the possibility that either E22 or D23 is involved in a salt bridge with another charged residue. If such a salt bridge exists and plays a critical role in aggregation, we would expect to see a similar effect when the other partner of the salt bridge is mutated. There are three positively charged residues in the Aβ42 sequence: R5, K16, and K28. R5R1 shows similar aggregation kinetics as that of the wild-type Aβ42, and K28R1 shows faster aggregation kinetics. Only K16R1 shows slower aggregation kinetics than wild-type Aβ42. However, K16R1 still shows a sigmoid aggregation curve, unlike E22 or D23. Therefore, our data suggest that E22 and D23 are not forming salt bridges with other positively charged residues. We propose that the role of E22 and D23 is to ensure this part of the protein is exposed to solvent because burial of two negative charges would be energetically unfavorable. Residues E22 and D23 are sites of several familial mutations, including E22G (Arctic),[38,39] E22K (Italian),[40,41] E22Q (Dutch),[42−44] E22Δ (Osaka),[45] and D23N (Iowa).[46] These familial mutants can be rationalized in a way that they reduce or neutralize the local charges and thus divert the Aβ aggregation from fibrillization to oligomerization pathways. This would produce more toxic oligomers and lead to early-onset Alzheimer's disease.

The six residue positions with aberrant aggregation kinetics include three glycine residues: G33, G37, and G38. Without side chains, glycine offers maximum backbone flexibility because glycine can be found almost anywhere on the Ramachandran plot.[47] There are a total of six glycine residues in Aβ sequence: G9, G25, G29, G33, G37, and G38. The four glycines at G25, G29, G33, and G37 comprise a GXXXG motif commonly found in transmembrane helices, called glycine zipper.[48] However, only mutations at two of these four glycine zipper positions resulted in delayed aggregation, suggesting that the mutations did not act on the formation of glycine zipper. Therefore, the importance of G33, G37, and G38 in aggregation is likely due to the backbone flexibility at these residue positions. Previously, Harmeier et al.[49] showed that G33I and G33A in Aβ42 displayed higher propensity to form higher oligomers. Fonte et al.[50]

DOI: 10.1021/acsomega.8b00887
ACS Omega 2018, 3, 8401−8407

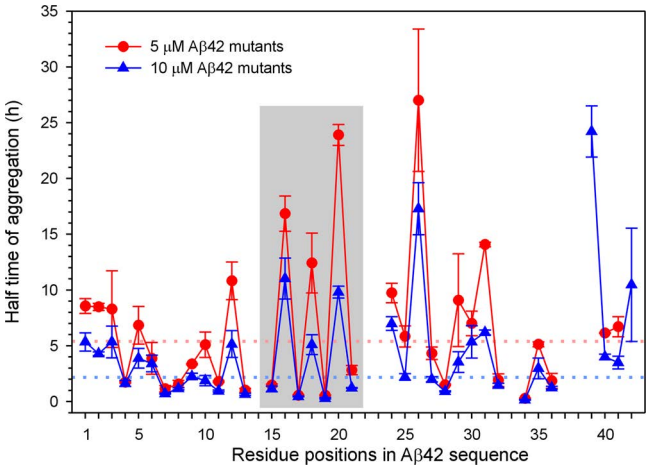

Figure 4. Plot of the half time of aggregation as a function of residue positions. Half time is defined as the time at which the thioflavin T fluorescence is at half of the fluorescence at the aggregation plateau and is determined directly from the kinetics curves. Each data point is an average of multiple repeats, and the error bars are the standard deviation. The gray box highlights residues 15−21, which show a periodicity of two in the half time of aggregation. Light red and light blue dotted lines denote the half time for wild-type Aβ42 at 5 and 10 μM, respectively.

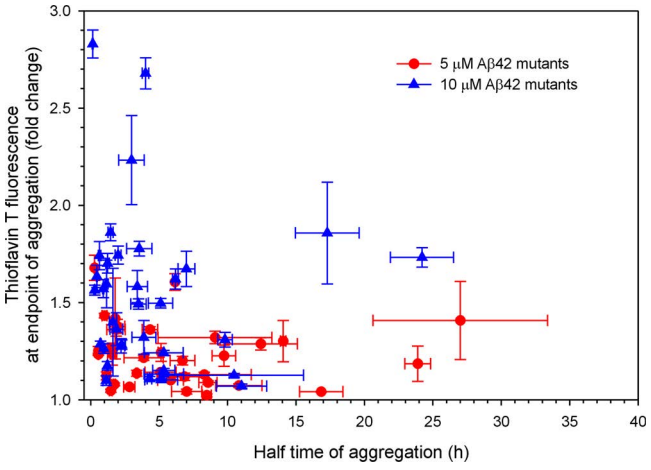

Figure 5. Plot of thioflavin T fluorescence at completion of aggregation versus the half time of aggregation. The thioflavin T fluorescence was measured at the end of aggregation, at which the aggregation time is at 40 h. Averages and standard deviations are calculated based on multiple repeats of aggregation experiments.

showed that the expression of G37L mutant of Aβ42 in *Caenorhabditis elegans* did not show detectable amyloid formation. These studies show that mutation to different amino acids can all affect fibril formation, supporting the notion that the role of these glycine residues in aggregation is primarily providing backbone flexibility.

There are three histidine residues in Aβ42 sequence: H6, H13, and H14. Only H14R1 shows markedly different aggregation kinetics, whereas H6R1 and H13R1 display typical sigmoidal aggregation curves. Previous structural studies using spin labeling and electron paramagnetic resonance suggest that H14 is part of a turn in Aβ42 fibrils.[25] Molecular dynamics studies of Aβ42 also consistently show a turn motif at residues 12−15.[51] Therefore, we suggest that the importance of H14 in Aβ42 fibrillization is likely to stabilize the turn around residue

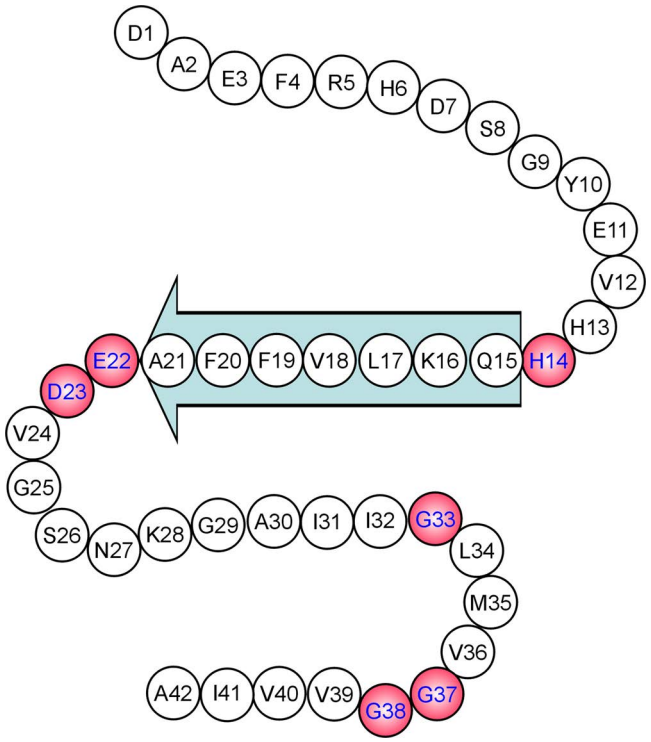

Figure 6. Summary of important structural features for Aβ42 fibril formation. Key residues are highlighted in pink. A potential β-strand region at residues 15−21 is represented by a block arrow.

14. Even though H13 is the adjacent residue and is of the same residue type, our data suggest that H13 and H14 play different roles in fibril nucleation and elongation. A mutagenesis study[52] using D-amino acids showed that D-histidine at position 14 caused substantial changes in Aβ42 aggregation, suggesting that the effect at H14 may also be related to the direction to which the H14 side chain is pointing.

Previously, Morimoto et al.[29] used the proline scanning mutagenesis approach to study the site-specific effect on Aβ42 aggregation. Proline is a β-strand breaker, and proline substitution at β-structure would presumably lead to reduced fibril formation. Out of 34 residue positions studied, Morimoto et al. identified three turn regions at residues 22−23, 33−34, and 38−39, which are insensitive to proline mutations. Interestingly, these residue positions coincide with the key residues (E22, D23, G33, G37, and G38) for Aβ42 aggregation that we identified in this work (Figure 6). In recent structural models of Aβ42 fibrils based on solid-state NMR[18,20,21] and cryoEM,[19] these key residues are not all located in turn regions, suggesting that structural features important for nucleation may be different from those for the final aggregation product, amyloid fibrils.

MATERIALS AND METHODS

Preparation of Aβ42 Proteins and Spin Labeling. Cysteine mutants of Aβ42 were introduced using the QuikChange site-directed mutagenesis kit (Agilent), and all mutations were confirmed with DNA sequencing. For protein expression, the plasmids containing Aβ42 constructs were transformed into *Escherichia coli* C41 cells, and the protein expression was induced with isopropyl β-D-1-thiogalactopyranoside as previously described.[25,53] Full-length Aβ was then cleaved from the fusion protein with Usp2-cc using previously published methods.[54] WT Aβ42 was buffer exchanged to 30 mM

DOI: 10.1021/acsomega.8b00887
ACS Omega 2018, 3, 8401−8407

NH_4 acetate (pH 10), lyophilized, and stored at −80 °C. For spin labeling, the spin labeling reagent (1-oxyl-2,2,5,5-tetramethylpyrroline-3-methyl methanethiosulfonate (MTSSL), AdipoGen Life Sciences) was used, and the detailed procedure has been previously published.[25,54] The spin-labeled Aβ42 proteins were then lyophilized and stored at −80 °C.

Aggregation Kinetics. Forty-three tubes of lyophilized powder corresponding to the wild-type and 42 spin-labeled Aβ42 mutants were dissolved in hexafluoroisopropanol (HFIP) to a final concentration of 100 μM and then incubated overnight with shaking at 1000 rpm. Then, HFIP was evaporated in the chemical hood at room temperature overnight. These samples were dissolved in 50 μL of CU buffer (20 mM CAPS, 8 M urea, pH 11). The wild-type Aβ concentration was determined using absorbance at 280 nm in CU buffer with an extinction coefficient of 1280 M cm^{-1}, which was previously determined in a denaturing buffer.[55] The spin-labeled Aβ concentration was determined using an extinction coefficient of 1740 M cm^{-1}, with the consideration of absorbance from disulfide bond and the nitroxide ring. Because Y10R1 does not have a tyrosine, the extinction coefficient of 460 M cm^{-1} was used. Then, Aβ stock solutions at 200 and 100 μM were made using CU buffer to dilute the original stock. For aggregation reaction, 2.5 μL of Aβ42 stock at either 200 or 100 μM was mixed with 42.5 μL of PBS (50 mM phosphate, 140 mM NaCl, pH 7.4) and 5 μL of thioflavin T (200 μM in PBS buffer). Therefore, each mutant of Aβ was aggregated at both 10 and 5 μM. Mutants H14R1, E22R1, D23R1, G33R1, G37R1, and G38R1 were also prepared at higher concentrations in CU buffer to set up aggregation at 20 and 40 μM with the same protocol of 20-fold dilution to PBS. To start aggregation, the 50 μL aggregation assay was transferred to a black 384-well Nonbinding Surface microplate with clear bottom (Corning product 3655) and sealed with a polyester-based sealing film (Corning product PCR-SP). The fluorescence was measured from the bottom with an excitation filter of 450 nm and an emission filter of 490 nm in a Victor 3V plate reader (Perkin Elmer). The aggregation was performed at 37 °C without agitation. The aggregation data are reported as fold change in fluorescence by dividing the average of thioflavin T fluorescence at each time point of measurement.

AUTHOR INFORMATION

Corresponding Author

*E-mail: zhefeng@ucla.edu. Phone: (310) 439-9843.

ORCID

Zhefeng Guo: 0000-0003-1992-7255

Author Contributions

†F.H. and G.P. contributed equally to this work.

Author Contributions

F.H. and G.P. designed and carried out experiments, analyzed data, and drafted the manuscript. Z.G. conceived and supervised the study, designed the experiments, and drafted the manuscript. All authors gave final approval for publication.

Notes

The authors declare no competing financial interest.

ACKNOWLEDGMENTS

Funding was provided by the National Institutes of Health (grant R01AG050687).

REFERENCES

(1) Chiti, F.; Dobson, C. M. Protein Misfolding, Amyloid Formation, and Human Disease: A Summary of Progress over the Last Decade. *Annu. Rev. Biochem.* **2017**, *86*, 27−68.

(2) Eisenberg, D.; Jucker, M. The Amyloid State of Proteins in Human Diseases. *Cell* **2012**, *148*, 1188−1203.

(3) Chatani, E.; Yamamoto, N. Recent Progress on Understanding the Mechanisms of Amyloid Nucleation. *Biophys. Rev.* **2018**, *10*, 527−534.

(4) Buell, A. K. The Nucleation of Protein Aggregates—From Crystals to Amyloid Fibrils. *Int. Rev. Cell Mol. Biol.* **2017**, *329*, 187−226.

(5) Kumar, E. K.; Haque, N.; Prabhu, N. P. Kinetics of Protein Fibril Formation: Methods and Mechanisms. *Int. J. Biol. Macromol.* **2017**, *100*, 3−10.

(6) Cohen, S. I. A.; Linse, S.; Luheshi, L. M.; Hellstrand, E.; White, D. A.; Rajah, L.; Otzen, D. E.; Vendruscolo, M.; Dobson, C. M.; Knowles, T. P. J. Proliferation of Amyloid-B42 Aggregates Occurs through a Secondary Nucleation Mechanism. *Proc. Natl. Acad. Sci. U.S.A.* **2013**, *110*, 9758−9763.

(7) Arosio, P.; Knowles, T. P. J.; Linse, S. On the Lag Phase in Amyloid Fibril Formation. *Phys. Chem. Chem. Phys.* **2015**, *17*, 7606−7618.

(8) Meisl, G.; Michaels, T. C. T.; Linse, S.; Knowles, T. P. J. Kinetic Analysis of Amyloid Formation. *Methods Mol. Biol.* **2018**, *1779*, 181−196.

(9) Meisl, G.; Kirkegaard, J. B.; Arosio, P.; Michaels, T. C. T.; Vendruscolo, M.; Dobson, C. M.; Linse, S.; Knowles, T. P. J. Molecular Mechanisms of Protein Aggregation from Global Fitting of Kinetic Models. *Nat. Protoc.* **2016**, *11*, 252−272.

(10) Selkoe, D. J.; Hardy, J. The Amyloid Hypothesis of Alzheimer's Disease at 25 Years. *EMBO Mol. Med.* **2016**, *8*, 595−608.

(11) Huang, Y.; Potter, R.; Sigurdson, W.; et al. Effects of Age and Amyloid Deposition on Aβ Dynamics in the Human Central Nervous System. *Arch. Neurol.* **2012**, *69*, 51−58.

(12) Pannee, J.; Portelius, E.; Oppermann, M.; Atkins, A.; Hornshaw, M.; Zegers, I.; Höjrup, P.; Minthon, L.; Hansson, O.; Zetterberg, H.; et al. A Selected Reaction Monitoring (SRM)-Based Method for Absolute Quantification of Aβ38, Aβ40, and Aβ42 in Cerebrospinal Fluid of Alzheimer's Disease Patients and Healthy Controls. *J. Alzheimer's Dis.* **2013**, *33*, 1021−1032.

(13) Kakuda, N.; Shoji, M.; Arai, H.; Furukawa, K.; Ikeuchi, T.; Akazawa, K.; Takami, M.; Hatsuta, H.; Murayama, S.; Hashimoto, Y.; et al. Altered γ-Secretase Activity in Mild Cognitive Impairment and Alzheimer's Disease. *EMBO Mol. Med.* **2012**, *4*, 344−352.

(14) Gravina, S. A.; Ho, L.; Eckman, C. B.; Long, K. E.; Otvos, L.; Younkin, L. H.; Suzuki, N.; Younkin, S. G. Amyloid β Protein (Aβ) in Alzheimer's Disease Brain. Biochemical and Immunocytochemical Analysis with Antibodies Specific for Forms Ending at Aβ40 or Aβ42(43). *J. Biol. Chem.* **1995**, *270*, 7013−7016.

(15) Iwatsubo, T.; Odaka, A.; Suzuki, N.; Mizusawa, H.; Nukina, N.; Ihara, Y. Visualization of Aβ42(43) and Aβ40 in Senile Plaques with End-Specific Aβ Monoclonals: Evidence That an Initially Deposited Species Is Aβ42(43). *Neuron* **1994**, *13*, 45−53.

(16) Mak, K.; Yang, F.; Vinters, H. V.; Frautschy, S. A.; Cole, G. M. Polyclonals to β-Amyloid(1−42) Identify Most Plaque and Vascular Deposits in Alzheimer Cortex, but Not Striatum. *Brain Res.* **1994**, *667*, 138−142.

(17) Miller, D. L.; Papayannopoulos, I. A.; Styles, J.; Bobin, S. A.; Lin, Y. Y.; Biemann, K.; Iqbal, K. Peptide Compositions of the Cerebrovascular and Senile Plaque Core Amyloid Deposits of Alzheimer's Disease. *Arch. Biochem. Biophys.* **1993**, *301*, 41−52.

(18) Colvin, M. T.; Silvers, R.; Ni, Q. Z.; Can, T. V.; Sergeyev, I. V.; Rosay, M.; Donovan, K. J.; Michael, B.; Wall, J. S.; Linse, S.; et al. Atomic Resolution Structure of Monomorphic Aβ42 Amyloid Fibrils. *J. Am. Chem. Soc.* **2016**, *138*, 9663−9674.

(19) Gremer, L.; Schölzel, D.; Schenk, C.; Reinartz, E.; Labahn, J.; Ravelli, R. B. G.; Tusche, M.; Lopez-Iglesias, C.; Hoyer, W.; Heise, H.; et al. Fibril Structure of Amyloid-ß(1-42) by Cryo-Electron Microscopy. *Science* **2017**, *358*, 116−119.

(20) Wälti, M. A.; Ravotti, F.; Arai, H.; Glabe, C. G.; Wall, J. S.; Böckmann, A.; Güntert, P.; Meier, B. H.; Riek, R. Atomic-Resolution

DOI: 10.1021/acsomega.8b00887
ACS Omega 2018, 3, 8401−8407

Structure of a Disease-Relevant Aβ(1-42) Amyloid Fibril. *Proc. Natl. Acad. Sci. U.S.A.* **2016**, *113*, E4976−E4984.
(21) Xiao, Y.; Ma, B.; McElheny, D.; Parthasarathy, S.; Long, F.; Hoshi, M.; Nussinov, R.; Ishii, Y. Aβ(1-42) Fibril Structure Illuminates Self-Recognition and Replication of Amyloid in Alzheimer's Disease. *Nat. Struct. Mol. Biol.* **2015**, *22*, 499−505.
(22) Hubbell, W. L.; López, C. J.; Altenbach, C.; Yang, Z. Technological Advances in Site-Directed Spin Labeling of Proteins. *Curr. Opin. Struct. Biol.* **2013**, *23*, 725−733.
(23) Nelson, R.; Sawaya, M. R.; Balbirnie, M.; Madsen, A. Ø.; Riekel, C.; Grothe, R.; Eisenberg, D. Structure of the Cross-Beta Spine of Amyloid-like Fibrils. *Nature* **2005**, *435*, 773−778.
(24) Zielke, V.; Eickmeier, H.; Hideg, K.; Reuter, H.; Steinhoff, H. J. A Commonly Used Spin Label: S-(2,2,5,5-tetramethyl-1-oxyl-Δ3-pyrrolin-3-ylmethyl) Methanethiosulfonate. *Acta Crystallogr., Sect. C: Cryst. Struct. Commun.* **2008**, *64*, o586−o589.
(25) Gu, L.; Tran, J.; Jiang, L.; Guo, Z. A New Structural Model of Alzheimer's Aβ42 Fibrils Based on Electron Paramagnetic Resonance Data and Rosetta Modeling. *J. Struct. Biol.* **2016**, *194*, 61−67.
(26) Wang, H.; Lee, Y. K.; Xue, C.; Guo, Z. Site-Specific Structural Order in Alzheimer's Aβ42 Fibrils. *R. Soc. Open Sci.* **2018**, *5*, No. 180166.
(27) Guo, Z.; Cascio, D.; Hideg, K.; Kálái, T.; Hubbell, W. L. Structural Determinants of Nitroxide Motion in Spin-Labeled Proteins: Tertiary Contact and Solvent-Inaccessible Sites in Helix G of T4 Lysozyme. *Protein Sci.* **2007**, *16*, 1069−1086.
(28) Guo, Z.; Cascio, D.; Hideg, K.; Hubbell, W. L. Structural Determinants of Nitroxide Motion in Spin-Labeled Proteins: Solvent-Exposed Sites in Helix B of T4 Lysozyme. *Protein Sci.* **2008**, *17*, 228−239.
(29) Morimoto, A.; Irie, K.; Murakami, K.; Masuda, Y.; Ohigashi, H.; Nagao, M.; Fukuda, H.; Shimizu, T.; Shirasawa, T. Analysis of the Secondary Structure of β-Amyloid (Aβ42) Fibrils by Systematic Proline Replacement. *J. Biol. Chem.* **2004**, *279*, 52781−52788.
(30) Meisl, G.; Yang, X.; Hellstrand, E.; Frohm, B.; Kirkegaard, J. B.; Cohen, S. I. A.; Dobson, C. M.; Linse, S.; Knowles, T. P. J. Differences in Nucleation Behavior Underlie the Contrasting Aggregation Kinetics of the Aβ40 and Aβ42 Peptides. *Proc. Natl. Acad. Sci. U.S.A.* **2014**, *111*, 9384−9389.
(31) Buell, A. K.; Galvagnion, C.; Gaspar, R.; Sparr, E.; Vendruscolo, M.; Knowles, T. P. J.; Linse, S.; Dobson, C. M. Solution Conditions Determine the Relative Importance of Nucleation and Growth Processes in α-Synuclein Aggregation. *Proc. Natl. Acad. Sci. U.S.A.* **2014**, *111*, 7671−7676.
(32) Šarić, A.; Buell, A. K.; Meisl, G.; Michaels, T. C. T.; Dobson, C. M.; Linse, S.; Knowles, T. P. J.; Frenkel, D. Physical Determinants of the Self-Replication of Protein Fibrils. *Nat. Phys.* **2016**, *12*, 874−880.
(33) Cohen, S. I. A.; Cukalevski, R.; Michaels, T. C. T.; Šarić, A.; Törnquist, M.; Vendruscolo, M.; Dobson, C. M.; Buell, A. K.; Knowles, T. P. J.; Linse, S. Distinct Thermodynamic Signatures of Oligomer Generation in the Aggregation of the Amyloid-β Peptide. *Nat. Chem.* **2018**, *10*, 523−531.
(34) Murphy, R. M. Kinetic Analysis of Aggregation Data. *Methods Mol. Biol.* **2013**, 201−217.
(35) Lee, J.; Culyba, E. K.; Powers, E. T.; Kelly, J. W. Amyloid-β Forms Fibrils by Nucleated Conformational Conversion of Oligomers. *Nat. Chem. Biol.* **2011**, *7*, 602−609.
(36) Fu, Z.; Aucoin, D.; Davis, J.; Van Nostrand, W. E.; Smith, S. O. Mechanism of Nucleated Conformational Conversion of Aβ42. *Biochemistry* **2015**, *54*, 4197−4207.
(37) Xue, C.; Lin, T. Y.; Chang, D.; Guo, Z. Thioflavin T as an Amyloid Dye: Fibril Quantification, Optimal Concentration and Effect on Aggregation. *R. Soc. Open Sci.* **2017**, *4*, No. 160696.
(38) Nilsberth, C.; Westlind-Danielsson, A.; Eckman, C. B.; Condron, M. M.; Axelman, K.; Forsell, C.; Stenh, C.; Luthman, J.; Teplow, D. B.; Younkin, S. G.; et al. The "Arctic" APP Mutation (E693G) Causes Alzheimer's Disease by Enhanced Aβ Protofibril Formation. *Nat. Neurosci.* **2001**, *4*, 887−893.
(39) Kamino, K.; Orr, H. T.; Payami, H.; Wijsman, E. M.; Alonso, M. E.; Pulst, S. M.; Anderson, L.; O'dahl, S.; Nemens, E.; White, J. A. Linkage and Mutational Analysis of Familial Alzheimer Disease Kindreds for the APP Gene Region. *Am. J. Hum. Genet.* **1992**, *51*, 998−1014.
(40) Tagliavini, F.; Tagliavini, F.; Rossi, G.; Padovani, C. V.; Magoni, M.; Andora, G.; Sgarzi, M.; Bizzi, C. A.; Savioardo, M.; Carella, F.; et al. A New βPP Mutation Related to Hereditary Cerebral Hemorrhage. *Alzheimer's Rep.* **1999**, *2*, S28.
(41) Bugiani, O.; Giaccone, G.; Rossi, G.; Mangieri, M.; Capobianco, R.; Morbin, M.; Mazzoleni, G.; Cupidi, C.; Marcon, G.; Giovagnoli, A.; et al. Hereditary Cerebral Hemorrhage with Amyloidosis Associated with the E693K Mutation of APP. *Arch. Neurol.* **2010**, *67*, 987−995.
(42) Levy, E.; Carman, M. D.; Fernandez-Madrid, I. J.; Power, M. D.; Lieberburg, I.; van Duinen, S. G.; Bots, G. T.; Luyendijk, W.; Frangione, B. Mutation of the Alzheimer's Disease Amyloid Gene in Hereditary Cerebral Hemorrhage, Dutch Type. *Science* **1990**, *248*, 1124−1126.
(43) Van Broeckhoven, C.; Haan, J.; Bakker, E.; Hardy, J. A.; Van Hul, W.; Wehnert, A.; Vegter-Van der Vlis, M.; Roos, R. A. Amyloid Beta Protein Precursor Gene and Hereditary Cerebral Hemorrhage with Amyloidosis (Dutch). *Science* **1990**, *248*, 1120−1122.
(44) Fernandez-Madrid, I.; Levy, E.; Marder, K.; Frangione, B. Codon 618 Variant of Alzheimer Amyloid Gene Associated with Inherited Cerebral Hemorrhage. *Ann. Neurol.* **1991**, *30*, 730−733.
(45) Tomiyama, T.; Nagata, T.; Shimada, H.; Teraoka, R.; Fukushima, A.; Kanemitsu, H.; Takuma, H.; Kuwano, R.; Imagawa, M.; Ataka, S.; et al. A New Amyloid β Variant Favoring Oligomerization in Alzheimer's-Type Dementia. *Ann. Neurol.* **2008**, *63*, 377−387.
(46) Grabowski, T. J.; Cho, H. S.; Vonsattel, J. P. G.; Rebeck, G. W.; Greenberg, S. M. Novel Amyloid Precursor Protein Mutation in an Iowa Family with Dementia and Severe Cerebral Amyloid Angiopathy. *Ann. Neurol.* **2001**, *49*, 697−705.
(47) Ho, B. K.; Brasseur, R. The Ramachandran Plots of Glycine and Pre-Proline. *BMC Struct. Biol.* **2005**, *5*, No. 14.
(48) Kim, S.; Jeon, T.-J.; Oberai, A.; Yang, D.; Schmidt, J. J.; Bowie, J. U. Transmembrane Glycine Zippers: Physiological and Pathological Roles in Membrane Proteins. *Proc. Natl. Acad. Sci. U.S.A.* **2005**, *102*, 14278−14283.
(49) Harmeier, A.; Wozny, C.; Rost, B. R.; Munter, L.-M.; Hua, H.; Georgiev, O.; Beyermann, M.; Hildebrand, P. W.; Weise, C.; Schaffner, W.; et al. Role of Amyloid-Beta Glycine 33 in Oligomerization, Toxicity, and Neuronal Plasticity. *J. Neurosci.* **2009**, *29*, 7582−7590.
(50) Fonte, V.; Dostal, V.; Roberts, C. M.; Gonzales, P.; Lacor, P.; Magrane, J.; Dingwell, N.; Fan, E. Y.; Silverman, M. A.; Stein, G. H.; et al. A Glycine Zipper Motif Mediates the Formation of Toxic β-Amyloid Oligomers in Vitro and in Vivo. *Mol. Neurodegener.* **2011**, *6*, No. 61.
(51) Tran, L.; Ha-Duong, T. Exploring the Alzheimer Amyloid-β Peptide Conformational Ensemble: A Review of Molecular Dynamics Approaches. *Peptides* **2015**, *69*, 86−91.
(52) Hayden, E. Y.; Hoi, K. K.; Lopez, J.; Inayathullah, M.; Condron, M. M.; Teplow, D. B. Identification of Key Regions and Residues Controlling Aβ Folding and Assembly. *Sci. Rep.* **2017**, *7*, No. 12434.
(53) Gu, L.; Liu, C.; Stroud, J. C.; Ngo, S.; Jiang, L.; Guo, Z. Antiparallel Triple-Strand Architecture for Prefibrillar Aβ42 Oligomers. *J. Biol. Chem.* **2014**, *289*, 27300−27313.
(54) Gu, L.; Liu, C.; Guo, Z. Structural Insights into Aβ42 Oligomers Using Site-Directed Spin Labeling. *J. Biol. Chem.* **2013**, *288*, 18673−18683.
(55) Edelhoch, H. Spectroscopic Determination of Tryptophan and Tyrosine in Proteins. *Biochemistry* **1967**, *6*, 1948−1954.

DOI: 10.1021/acsomega.8b00887
ACS Omega 2018, 3, 8401−8407